ELSEVIER

Journal of Alloys and Compounds 330–332 (2002) 855–860

Journal of ALLOYS AND COMPOUNDS

www.elsevier.com/locate/jallcom

The phase structure and electrochemical properties of the melt-spun alloy $Zr_{0.7}Ti_{0.3}Mn_{0.4}V_{0.4}Ni_{1.2}$

S.K. Zhang[a], Q.D. Wang[a,*], Y.Q. Lei[a], G.L. Lü[b], L.X. Chen[a], F. Wu[c]

[a]*Department of Materials Science and Engineering, Zhejiang University, Hangzhou, 310027, PR China*
[b]*Central Laboratory, Zhejiang University, Hangzhou, 310028, PR China*
[c]*National Engineering Development Center of High Technology Energy-storage Materials, Zhongshan, 528437, PR China*

Abstract

The crystal structure, phase abundance, microstructure and electrochemical properties of the AB_2-type Laves phase hydrogen storage alloy $Zr_{0.7}Ti_{0.3}Mn_{0.4}V_{0.4}Ni_{1.2}$ were studied, prepared both by arc-melting and melt-spinning. The XRD patterns have revealed that two Laves phases, C14 and C15 are formed in the as-cast alloy. In the melt-spun alloy, besides the C14 and C15 phase in very fine crystal grains, there appears a new crystalline C14 phase with very fine crystallites, which is named the nanocrystallite C14 in this paper. SEM and EDS analyses have indicated that the microstructure of melt-spun alloy is a very fine dendritic structure (10×3 μm), while the as-cast alloy is a much coarser dendritic structure (300×50 μm) with noticeable composition segregation. Electrochemical tests have indicated that the melt-spun alloy has a higher discharge capacity of 385 mA h g^{-1} in comparison with 371 mA h g^{-1} for the as-cast alloy and the melt-spun alloy has very good cycling stability. After 500 cycles, 80.7% of the initial discharge capacity is retained, much higher than 63.1% of the as-cast alloy. It is thus inferred that the electrochemical capacity of the nanocrystallite C14 phase is higher than that of the conventional C14 phase. Nevertheless, the activation property and the high-rate dischargeability of the melt-spun alloy were both found to decrease noticeably, most probably due to the higher resistance against decrepitation and cracking of the alloy with a more refined grain structure.

Keywords: Phase structure; Micro-structure; Electrochemical properties; Melt-spun electrode alloy; (Zr,Ti)-based Laves phase alloy

1. Introduction

AB_2-type Laves phase hydrogen storage alloys are promising negative electrode materials for Ni/MH storage batteries, because they have a higher electrochemical discharge capacity than the prevailing AB_5-type mischmetal-based alloys. Yet the AB_2-type Laves phase alloys are multi-phase alloys. Their electrochemical properties are very closely related to the phase structure, phase abundance and microstructures of the alloys. Only when the rules and conditions for the formation of different phases and structures and the electrochemical properties of each phase and structure are well known, one will be able to use this type of alloy more wisely and successfully. Endeavor has recently been made in this direction [1–3]. In our previous studies, the effect of material processing including heat treatment [4,5] and rapid quenching [6,7] on the phase composition, micro-structure and the electrochemical properties of the Zr-based Laves phase alloy were studied. We discovered that a micro-crystallite C14 phase besides the regular C14 and C15 Laves phases was formed during rapid quenching (melt-spinning) and affected the properties of the alloy $Zr(Ni_{0.55}V_{0.1}Mn_{0.3}Cr_{0.55})_2$ [6,7], for which the main phase in the as-cast state was the C15 Laves phase.

In this investigation, the (Zr-Ti)-based $Zr_{0.7}Ti_{0.3}Mn_{0.4}V_{0.4}Ni_{1.2}$ alloy, in which the C14 phase is its main phase, has been chosen and the phase structure, phase abundance, microstructure and electrochemical properties of the alloy in both as-cast and melt-spun state were studied, and the results analyzed and discussed.

2. Experimental details

$Zr_{0.7}Ti_{0.3}Mn_{0.4}V_{0.4}Ni_{1.2}$ alloy samples were prepared by arc melting on a water-cooled copper hearth under argon atmosphere. Samples were turned over and remelted four times to ensure higher homogeneity. The purity of the metallic elements Zr, Ti, Ni, V, Mn used for sample preparation was all higher than 99.9%. Part of the as-cast

*Corresponding author.

0925-8388/02/$ – see front matter
PII: S0925-8388(01)01482-7

alloy was subsequently remelted and quenched by the melt-spinning method. The cooling rate of the melt-spun ribbon was estimated to be 10^{-5} K s^{-1}.

Alloy samples were ground into powder, below 300 mesh for electrochemical and X-ray diffraction (XRD) measurements. Electrode pellets 10 mm in diameter were prepared by cold pressing a mixture of alloy powder (about 100 mg) and powdered electrolytic copper (44 μm) in a mass ratio of 1:2. Electrochemical measurements were carried out at 25°C in a tri-electrode half cell with $Ni(OH)_2$/NiOOH as the counter electrode and Hg/HgO as the reference electrode, in a 6 M KOH electrolyte, with the same procedure as reported previously [8].

The phase structure of the samples was determined by XRD analysis using the Rikagu D/Max-313 X-ray diffractometer with Cu Kα radiation. The continuous scanning speed was 4° min^{-1}, and the 2θ range was 20–120°. The results were analyzed with the Rietveld method [9]. The microstructure and the composition of the samples were investigated using a Philips-XL30 scanning electron microscope (SEM) and EDS.

3. Results and discussion

3.1. XRD and SEM analysis

Fig. 1 shows the XRD patterns of the as-cast and melt-spun alloys. In Fig. 1(a) the profile indicates that the as-cast alloy is composed of C14 and the C15 Laves phases. For the melt-spun alloy (Fig. 1(b)) according to the Rietveld software Rietquan [11], besides the C14 and C15 Laves phases, the characteristic broadening of the bottom part of the C14-phase, particularly at the bottom part of the peak (103) of the C14 phase, shows the presence of the third phase in the form of very small crystallites, which is named nanocrystallite C14 phase in this paper. Meanwhile the diffraction peaks of the C15 Laves phase remain sharp after rapid solidification.

The lattice constants and the phase composition of the two differently prepared alloys determined from the XRD Rietveld analysis are summarized in Table 1, from which it can be seen that due to rapid solidification, the C15 phase abundance decreases from 16.3 to 11.9 wt.%, and the phase abundance of the regular C14 phase decreases from 83.7 to 62.3 wt.% with the appearance of 25.8 wt.% nanocrystallite C14 phase. The melt-spinning process makes the lattice constants a and cell volume (V) of the C15 Laves phase increase, while the a, c and V of the regular C14 Laves phase decreased with a small change in the a/c ratio. The a/c ratio of the nanocrystallite C14 phase is much smaller and its cell volume much larger than those of the regular C14 phase.

Table 2 shows the crystallite size and micro-strain of the melt-spun and the as-cast $Zr_{0.7}Ti_{0.3}Mn_{0.4}V_{0.4}Ni_{1.2}$ alloy samples. We can see from this that the crystallites of the new C14 phase are much smaller in size compared with the size of the crystallites of the C15 and regular C14 phase of both the as-cast and the melt-spun state. The reason for the smaller crystallite size of the as-cast alloy in comparison with that of the melt-spun alloy is probably due to the appearance of new substructures during the slower solidification.

When compared with the results of our previous investigations [3,4,6], we find that as before, a new phase, the nanocrystallite C14 phase, appears at the expense of the C15 and regular C14 phase when subjected to rapid solidification, but the lattice parameters, the a/c ratio and the cell volume of the new phase formed are different for the Zr-based alloy and the (Zr,Ti)-based alloys. For the nanocrystallite C14 phase of Zr-based Laves phase alloy formed in melt-spinning, a/c is increased and the cell volume is decreased, while for the new C14 phase in (Zr,Ti)-based Laves phase alloy, a/c decreases and the cell volume increases. From these results we believe that rapid solidification always favors the formation of the nanocrystallite C14 phase with very small crystallite size, but the lattice parameters and the cell volume vary greatly with composition. It is this difference that makes the electrochemical properties of the nanocrystallite C14 phase different in alloys with different compositions.

Fig. 2(a) shows the SEM micrograph of an as-cast sample. The micro-structure of the as-cast alloy is of a coarser dendritic structure. The average size of the columnar grain is around 300×50 μm. Fig. 2(b) shows the micro-structure of the region of the secondary branches of the as-cast alloy, in which the composition segregation is very pronounced. Fig. 2(c) shows the microstructure of the melt-spun alloy. It can be seen from the picture that the alloy is of much finer dendritic structure. The average size of each grain is about 10×3 μm with a lower degree of segregation. Morphologically, we cannot distinguish the three phases on the SEM micrograph. Some work is being done on it with TEM and will be published soon. Fig. 3(a,b) shows the EDS results for sites every 1 μm apart along a straight line on the surface of the alloy specimens. The results indicate that the distribution of Ni and Zr of the as-cast alloy is less uniform, the Ni fluctuates from 45.5 to 63.3 at.%, and the Zr fluctuates from 10.5 to 24.2 at.% (with higher Ni and lower Zr for C14 phase), deviating noticeably from the nominal composition (Zr: 23.3 at.%, Ni: 40 at.%). For the melt-spun alloy the content of each element is much more uniform than for the as-cast alloy. The content of Ni varies from 36.6 to 42.5 at.%, and that of Zr from 20.5 to 24.2 at.%, much closer to the nominal composition (still with higher Ni and lower Zr for the C14 phase). The fluctuation of the content of other elements including Mn, V and Ti is also greater for the as-cast and smaller for the melt-spun alloy. This indicates that the melt-spinning process effectively reduces the dendritic composition segregation in the alloy.

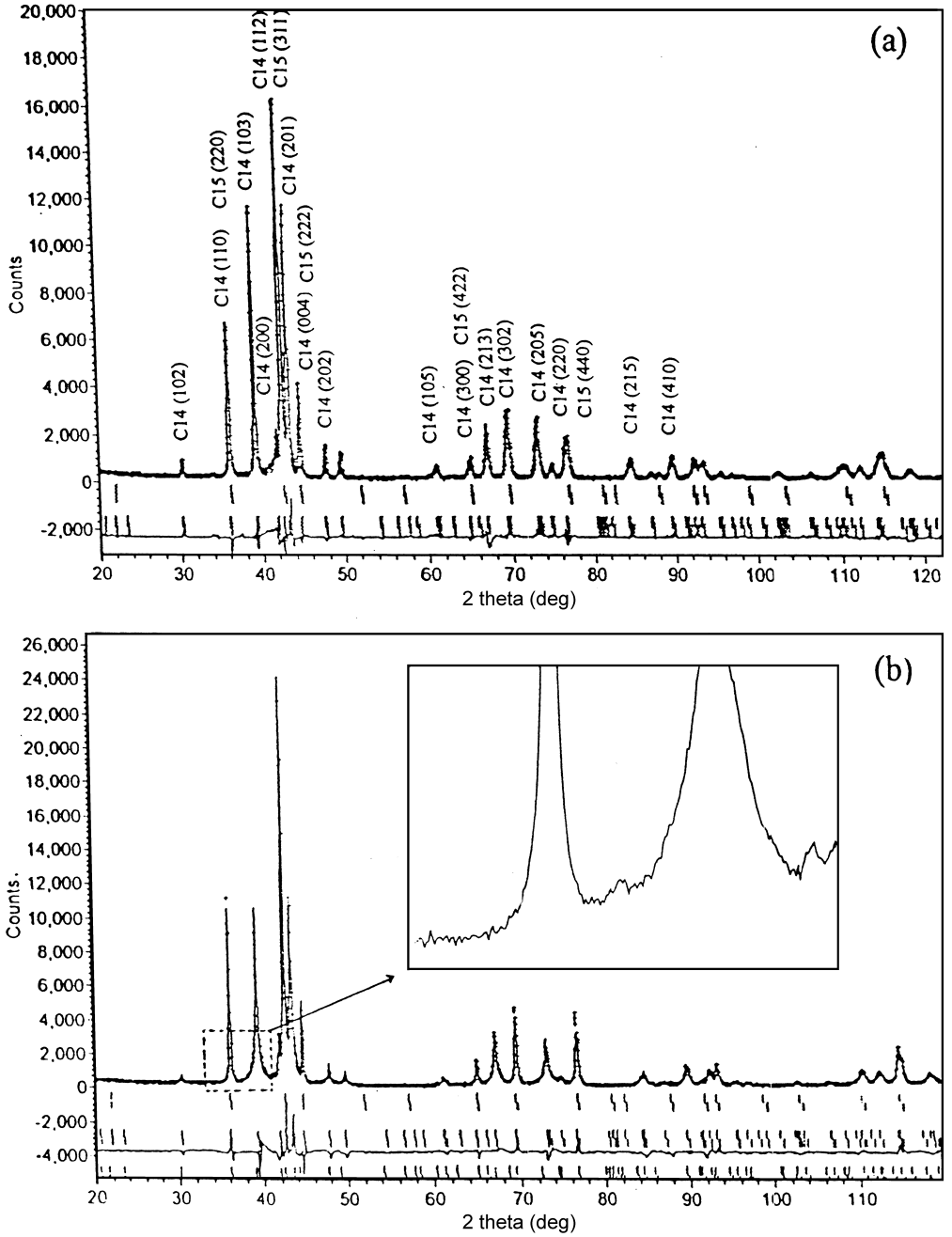

Fig. 1. The XRD patterns of the two differently prepared $Zr_{0.7}Ti_{0.3}Mn_{0.4}V_{0.4}Ni_{1.2}$ samples; (a) as-cast and (b) melt-spun alloy.

Table 1
The lattice parameters and phase abundance of melt-spun and as-cast $Zr_{0.7}Ti_{0.3}Mn_{0.4}V_{0.4}Ni_{1.2}$ samples

Alloy	Phase composition		Lattice constants			
	Phase	Phase abundance (wt.%)	a (nm)	c (nm)	a/c	Cell volume (V) (nm^3)
As-cast	C15	16.28 (0.36)	0.70099 (02)			0.34445
	C14	83.72 (1.08)	0.49771 (02)	0.81132 (03)	0.6134	0.17405
Melt-spun	C15	11.91 (0.90)	0.70241 (01)			0.34655
	C14	62.25 (1.30)	0.49705 (05)	0.80999 (05)	0.6136	0.17330
	Nano-C14	25.84 (0.88)	0.49643 (50)	0.82113 (53)	0.6046	0.17529

Table 2
The crystallite size and micro-strain of the melt-spun and as-cast $Zr_{0.7}Ti_{0.3}Mn_{0.4}V_{0.4}Ni_{1.2}$ samples

Alloy	Phase					
	C15		C14		Nano-C14	
	Crystallite size (nm)	$\langle\epsilon^2\rangle^{1/2}$ ($\times10^{-4}$)	Crystallite size (nm)	$\langle\epsilon^2\rangle^{1/2}$ ($\times10^{-4}$)	Crystallite size (nm)	$\langle\epsilon^2\rangle^{1/2}$ ($\times10^{-4}$)
As-cast	42.0	3.75	49.4	17.6	–	–
Melt-spun	65.2	7.51	51.5	11.4	3.69	2.51

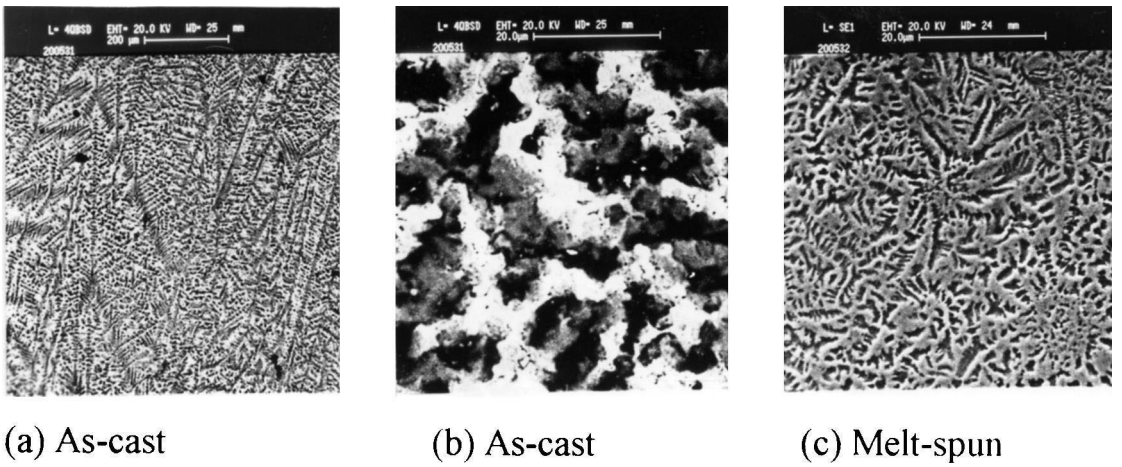

Fig. 2. The SEM morphology of the as-cast and melt-spun $Zr_{0.7}Ti_{0.3}Mn_{0.4}V_{0.4}Ni_{1.2}$ alloys; (a) and (b) the as-cast alloy, (c) the melt-spun alloy.

3.2. Electrochemical properties

Fig. 4 shows the activation curves of the as-cast and melt-spun alloys. It can be seen that the as-cast alloy is activated much more easily than the melt-spun alloy. It takes 25 charge–discharge cycles for the melt-spun alloy to reach its highest capacity, while the as-cast alloy only needs 13 cycles. The maximum discharge capacity of the melt-spun alloy is 385 mA h g^{-1}, slightly higher than the 371 mA h g^{-1} for the as-cast alloy. From the variation in phase composition between the as-cast and the melt-spun alloys, since only the phase abundance of the nanocrystal-

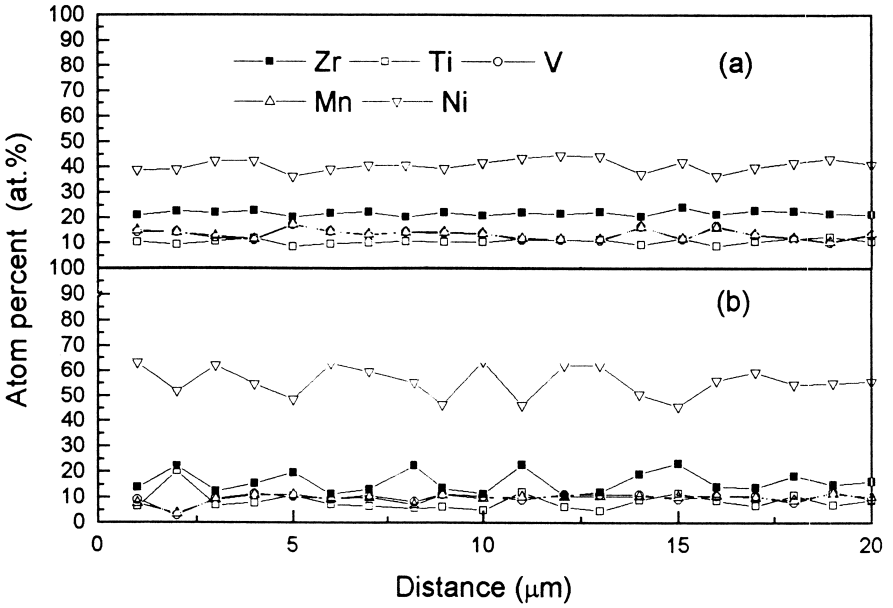

Fig. 3. The EDS results for sites along a straight line on the surface of melt-spun alloy (a) and as-cast alloy (b).

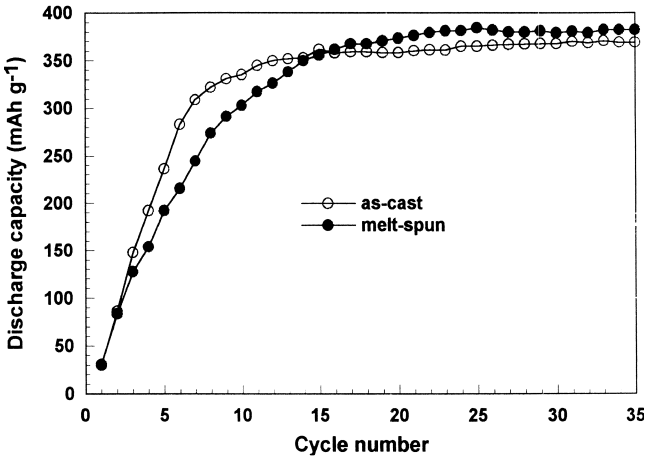

Fig. 4. The activation process of the differently prepared $Zr_{0.7}Ti_{0.3}Mn_{0.4}V_{0.4}Ni_{1.2}$ alloy sample curves.

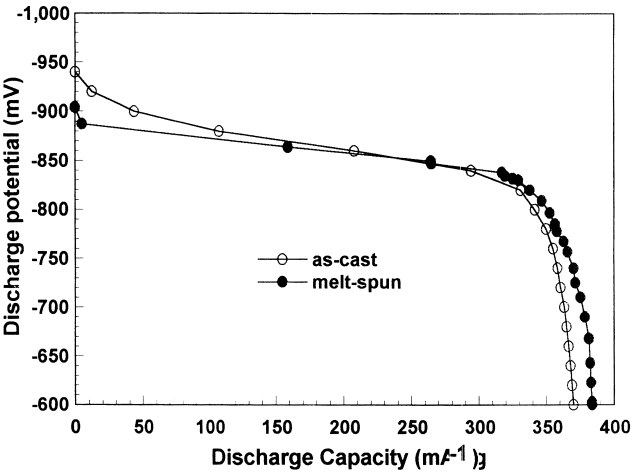

Fig. 5. The discharge potential curves of the $Zr_{0.7}Ti_{0.3}Mn_{0.4}V_{0.4}Ni_{1.2}$ alloy samples.

lite C14 phase is increased from 0 to 25.8 wt.% while the phase abundance of the conventional C14 and C15 phase both are decreased, the higher discharge capacity of the melt-spun alloy (384 mA h g^{-1}) can only be attributed to the higher discharge capacity of the nanocrystalline C14 phase than the conventional C14 phase. The increase in the discharge capacity of the nanocrystallite C14 phase over the regular C14 phase is a special feature of the (Zr,Ti)-based AB_2-type Laves phase hydrogen storage alloy. For the Zr-based alloys studied previously [7], the discharge capacity of the nanocrystallite phase is smaller, as the maximum discharge capacity decreases with the rate of rapid quenching and the increase in amount of nanocrystallite C14 phase formed in melt-spinning. One evident difference between these two nanocrystalline C14 phases is the variation of crystal volume during melt-spinning. For the (Zr,Ti)-based alloy in this study, the nanocrystallite C14 phase is found to have a cell volume augmentation during melt-spinning, while the nanocrystallite phase was found to have a volume reduction during melt-spinning for the Zr-base alloy [6,7]. We believe the increase in cell volume of the nanocrystalline C14 phase to be the reason for the augmentation in its electrochemical capacity, as it is well known that the hydrogen storage alloy with a larger cell volume absorbs hydrogen more readily [10].

Fig. 5 shows the discharge potential curves of the two alloys at the discharge current density of 50 mA h g^{-1}. It can be seen that slope of the discharge potential curve for the melt-spun alloy is less steep than that of the as-cast alloy and the average discharge potential of the melt-spun alloy is slightly lower. It is generally accepted that the slope of the discharge potential-discharge capacity curve is influenced by the homogeneity of the alloy composition. The more homogeneous the alloy, the flatter is the slope of the discharge potential plateau. This result indicates that the melt-spinning process enhances the compositional homogeneity of the alloy, and is in agreement with the EDS results in Fig. 3.

Fig. 6 shows the electrochemical cycling stability of the two alloys. The result indicates that the cycling stability of melt-spun alloy is much higher than that of the as-cast alloy. After 500 charge–discharge cycles, the capacity retention rate of the melt-spun alloy is 81%, while that of the as-cast alloy is only 63%. The high-rate dischargeability of as-cast alloy is 78%, superior to 58% of melt-spun alloy. Some important electrochemical properties of the two differently processed alloys are summarized in Table 3.

The degradation of the activation property and the high rate dischargeability of the melt-spun alloy cannot be well interpreted simply from the reduction in grain size and the appearance of nanocrystallite C14 phase in the form of very fine crystallites. If no other important factors influence the reaction, with the reduction in grain size, the paths for the migration of hydrogen atoms and the active

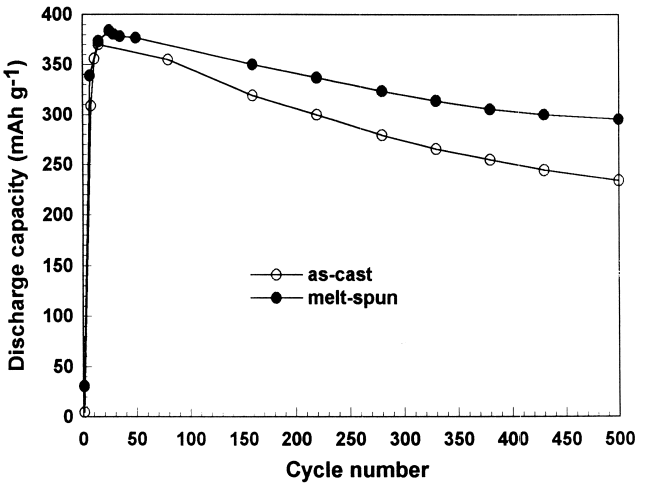

Fig. 6. The cycling curves of the two differently prepared $Zr_{0.7}Ti_{0.3}Mn_{0.4}V_{0.4}Ni_{1.2}$ samples.

Table 3
The electrochemical properties of the melt-spun and as-cast alloys of $Zr_{0.7}Ti_{0.3}Mn_{0.4}V_{0.4}Ni_{1.2}$

Alloy	C_{max} (mA h g^{-1})	Activation property (cycle)	Rate of capacity retention rate after 300 and 500 cycles (%)		High-rate dischargeability (%)
			S_{300}	S_{500}	
As-cast	371	13	75.4	63.1	77.9
Melt-spun	385	25	83.3	80.7	57.7

sites for electrochemical reaction on the surface in the grain boundaries should be increased and the experimental result should have been reversed. That makes us believe that the determining factor for the activation as well as for the high-rate dischargeability is the surface exposed directly to the KOH electrolyte. New surfaces are generated only when the grains of the electrode alloy crack or decrepitate during cycling due to volume expansion during hydriding or charging. As the crystal grains of a melt-spun alloy are much smaller in comparison with the grains of an as-cast alloy, the strain energy generated during hydriding can be transmitted to the grain boundaries and thus dissipated more readily. That makes the alloy particles decrepitate less readily. Since the fresh surface exposed to the electrolyte is greatly reduced in each cycle, the melt-spun alloy is activated much more slowly and is electrochemically less active for high rate discharging. The same reason can be used to explain the higher cycling stability of the melt-spun alloy. The other reason for the higher cycling stability is the higher compositional homogeneity of the melt-spun alloy, which leads to less local cell reactions on the surface of the alloy in contact with the electrolyte.

4. Conclusions

1. The as-cast $Zr_{0.7}Ti_{0.3}Mn_{0.4}V_{0.4}Ni_{1.2}$ alloy is composed of C14 and C15 phases. Melt-spinning refines the micro-structure and reduces the size of crystal grains greatly. In the meantime, a new nanocrystallite C14 phase appears.
2. The electrochemical capacity of the electrode of melt-spun alloy $Zr_{0.7}Ti_{0.3}Mn_{0.4}V_{0.4}Ni_{1.2}$ is slightly higher (385 mA h g^{-1}) than that of the as-cast alloy (371 mA h g^{-1}). This is believed to be due mainly to the higher discharge capacity of the nanocrystallite C14 phase.
3. The cycling stability of the melt-spun alloy is much improved, due to the lower cracking and decrepitation of alloy grains during cycling.
4. For the same reason of less decrepitation and cracking, the activation property and high-rate dischargeability of the melt-spun alloy is degraded.

Acknowledgements

This work is supported by the National Advanced Materials Committee of China (project number 863-715-004-0060).

References

[1] T. Okawa, T. Yao, Y. Moriwaki et al., Natl. Tech. Rep. 40 (4) (1994) 476–491.
[2] B. Knosp, C. Jordy, P. Blanchard et al., J. Electrochem. Soc. 145 (5) (1998) 1478–1482.
[3] H.J. Chuang, S.S. Huang, C.Y. Ma, S.L.I. Chan, J. Alloys Comp. 285 (1997) 284.
[4] Q.A. Zhang, Y.Q. Lei, X.G. Yang, K. Ren, Q.D. Wang, J. Alloys Comp. 292 (1999) 236–240.
[5] Q.A. Zhang, Y.Q. Lei, X.G. Yang, K. Ren, Q.D. Wang, J. Alloys Comp. 292 (1999) 241–246.
[6] G.L. Lü, K.Y. Shu, L.S. Chen, X.Y. Song, X.G. Yang, Y.Q. Lei, Q.D. Wang, J. Alloys Comp. 293–295 (1999) 107–112.
[7] K.Y. Shu, Y.Q. Lei, X.G. Yang, G.F. Lin, Q.D. Wang, G.L. Lü, J. Alloys Comp. 293–295 (1999) 756–761.
[8] Y.Q. Lei, Z.P. Li, C.P. Chen, J. Wu, Q.D. Wang, J. Less-Common Met. 172–174 (1991) 1205.
[9] K.Y. Shu, Y.Q. Lei, X.G. Yang, S.K. Zhang, L.S. Chen, G.L. Lü, Q.D. Wang, J. Alloys Comp. 290 (1999) 124–128.
[10] C.E. Lundin, F.E. Lynch, C.M. Magee, J. Less-Common Met. 56 (1977) 19.
[11] L. Lutterotli, P. Scardi, J. Appl. Crystallogr. 23 (1990) 246–252.